ELSEVIER

Surface Science 498 (2002) 321–336

SURFACE SCIENCE

www.elsevier.com/locate/susc

Adhesion, stability, and bonding at metal/metal-carbide interfaces: Al/WC

Donald J. Siegel [a,*,1], Louis G. Hector Jr. [b,2], James B. Adams [c,3]

[a] *Department of Physics, University of Illinois at Urbana-Champaign, 1110 West Green St., Urbana, IL 61801, USA*
[b] *Surface Science Division, ALCOA Technical Center, ALCOA Center, PA 15069-0001, USA*
[c] *Chemical and Materials Engineering Department, Arizona State University, Tempe, AZ 85287-6006, USA*

Received 5 July 2001; accepted for publication 29 October 2001

Abstract

We examine the relative stability and adhesion of the polar Al(1 1 1)/WC(0 0 0 1) interface using density functional theory. Relaxed atomic geometries and the ideal work of adhesion were calculated for six different interfacial structures, taking into account both W- and C-terminations of the carbide. The interfacial electronic structure was analyzed to determine the nature of metal/carbide bonding. Based on the surface and interfacial free energies, we find that both the clean WC(0 0 0 1) surface and the optimal interface geometry are W-terminated. Although both terminations yield substantial adhesion energies in the range 4–6 J/m^2, bonding at the optimal C-terminated structure is nearly 2 J/m^2 stronger, consistent with an argument based on surface reactivity. In addition, we examine the effects of Li and Mg alloying elements at the interface, and find that they result in a strain-induced reduction of metal–ceramic adhesion.

Keywords: Density functional calculations; Computer simulations; Adhesion; Surface energy; Tribology; Aluminum; Carbides

1. Introduction

Interfaces between metals and ceramics play a vital role in an increasingly large number of industrial applications [1]: heterogeneous catalysis, microelectronics, thermal barriers, corrosion protection and metals processing are but a few representative examples. However, experimental complications associated with the study of a buried interface, and theoretical difficulties arising from complex interfacial bonding interactions have hindered the development of general, analytic models capable of accurately predicting fundamental interfacial quantities.

One such quantity which is key to predicting the mechanical properties of an interface is the ideal work of adhesion, W_{ad} [1], which is defined as the bond energy needed (per unit area) to reversibly separate an interface into two free surfaces, neglecting plastic and diffusional degrees of freedom.

* Corresponding author.
E-mail address: djsiege@sandia.gov (D.J. Siegel).
[1] Present address: Sandia National Laboratories, Mail Stop 9161, Livermore, CA 94551, USA.
[2] Present address: General Motors R&D Center, Mail Code 480-106-224, 30500 Mound Road, Warren, MI 48090-9055, USA.
[3] Visit: http://ceaspub.eas.asu.edu/cms.

0039-6028/01/$ - see front matter
PII: S0039-6028(01)01811-8

For example, the degree of plastic deformation which occurs during interfacial fracture is known to depend upon $\mathscr{W}_{ad}$ [2–4]. Formally, $\mathscr{W}_{ad}$ can be defined in terms of either the surface and interfacial energies (relative to the respective bulk materials) or by the difference in total energy between the interface and its isolated slabs:

$$\mathscr{W}_{ad} = \sigma_{1v} + \sigma_{2v} - \gamma_{12} = \left(E_1^{tot} + E_2^{tot} - E_{12}^{tot}\right)/A. \quad (1)$$

Here σ_{iv} is the surface energy of slab i, γ_{12} is the interface energy, E_i^{tot} is the total energy of slab i, and E_{12}^{tot} is the total energy of the interface system. The total interface area is given by A.

Although there has recently been much activity aimed at understanding metal/oxide interfaces [1,5–12], much less is known about metal/ceramic adhesion involving non-oxide ceramics. Within this class, the transition metal carbides and nitrides are a particularly notable omission, considering their exceptional hardness, strength, and corrosion resistance [13]. To our knowledge, there have been only two studies of adhesion between metals and transition metal carbides/nitrides based on density functional theory (DFT) [14,15], along with a few earlier studies [16–18] performed using semi-empirical methods. Hartford [19] calculated the interfacial free energy of the Fe/VN system, including the effects of N vacancies. The interface energy was found to be negative for all systems consisting of more than one VN layer, with the presence of vacancies resulting in a small increase in interfacial energy. The interfacial bonds were determined to consist mainly of covalent N(p)–Fe(d) σ interactions, with minor V(d)–Fe(d) character. Secondly, Dudiy et al. [20] examined the Co/TiC interface, and found that their calculated $\mathscr{W}_{ad}$ values agreed with wetting experiments to within 10%. The dominant bonding mechanism involved strong "metal-modified" covalent Co–C bonds.

We are not aware of any theoretical studies which examine adhesion of Al to transition metal carbides/nitrides. However, two groups have used DFT to study interfaces of Al with other non-oxide ceramics. Hoekstra and Kohyama [21] considered the polar Al/β-SiC(0 0 0 1) interface, and found relatively large adhesion energies of 6.42 and 3.74 J/m^2 for both C and Si terminations, respectively. Conversely, a relatively weak adhesion of about 0.9 J/m^2 was found for the Al/AlN system by Ogata and Kitagawa [22]. On the experimental side, several groups (see Ref. [23] for a recent review) have investigated the wettability of ceramic substrates by various metals. Although the wettability of WC has been examined for a few interfaces involving mainly transition metals [24] and group IV elements [25], data pertaining to interfaces with Al is lacking.

In this work we present the first theoretical investigation of *any* metal/WC interface, focusing on Al/WC. Tungsten carbide is widely used in tribological applications as a wear-resistant coating for the purposes of reducing adhesion. However, the factors which determine the adhesive properties of a given coating are still poorly understood, and the evaluation of many coatings is often performed on a trial-and-error basis. At the other extreme, in microelectronics packaging there is generally a need for *strong* adhesion between a carbide/nitride layer and a metallic interconnect or SiO_2. Since the mechanical properties of an interface depend sensitively upon the detailed atomic and electronic structure at the junction, knowledge of this type would be a valuable tool in optimizing the performance of these, and other, systems.

The goal of the present work is to calculate the electronic structure, $\mathscr{W}_{ad}$, optimal geometries, and the interface stability of several representative polar Al/WC interfaces within a first-principles framework in order to better understand the nature of metal/ceramic adhesion. Previous studies have shown this approach to be reliable in reproducing $\mathscr{W}_{ad}$ values from experiment [1,7,8,20]. The Al/WC system serves as a convenient model of simple-metal/transition metal carbide adhesion, in that both polar and non-polar interfaces may be considered with moderately sized simulation cells resulting from similar lattice geometries. Our emphasis here is on the polar Al(1 1 1)/WC(0 0 0 1) geometry; the Al(1 1 0)/WC(1 1 $\bar{2}$ 0) system is discussed elsewhere [26].

The remainder of this paper is organized as follows: Section 2 describes the computational

methodology used in this study. Section 3 presents the results of our bulk and surface calculations on the pure materials. The major results of this paper are presented in Section 4, where we discuss the interfacial stability, adhesion, electronic structure, and the effects of alloys on the Al/WC metal–ceramic interface. Finally, we summarize our findings in Section 5.

2. Methodology

For this study we employ DFT [14,15], as implemented in the Vienna ab initio simulation package (VASP) [27]. VASP uses a plane-wave basis set for the expansion of the single particle Kohn–Sham wave functions, and pseudopotentials [28,29] to describe the computationally expensive electron–ion interaction. The ground state charge density and energy are calculated using a preconditioned conjugate gradient minimization algorithm [30,31] coupled with a Pulay-like mixing scheme [32–34]. Sampling of the irreducible wedge of the Brillouin zone is performed with a regular Monkhorst–Pack grid of special **k**-points [35]. Due to numerical instabilities associated with integrating the step-function character of the 0 K Fermi–Dirac distribution, partial occupancies of the single-particle wave functions are introduced [36,37] with an energy level broadening of 0.1 eV. Ground state atomic geometries were obtained by minimizing the Hellman–Feynman forces [38,39] using either a conjugate gradient [30] or quasi-Newton [32] algorithm. Finally, two separate approximations to the exchange-correlation energy were employed: the traditional local density approximation (LDA) as parameterized by Perdew and Zunger [40], and the generalized gradient approximation (GGA) of Perdew et al. [41] (PW91). More detailed descriptions of VASP can be found in the literature [27].

Due to the substantial computational cost of performing a DFT calculation on supercells containing first row and transition metal elements, we emphasize that our molecular statics (0 K) predictions of structure and adhesion energies do not account for temperature and larger-scale size effects such as reconstructions and lattice mismatch.

3. Bulk and surface calculations

3.1. Bulk properties

To assess the accuracy of the pseudopotential approximation and the importance of gradient corrections to exchange and correlation effects, we have performed a series of calculations on the bulk Al and WC phases. Results for Al were presented in an earlier study of the Al/α-Al_2O_3 interface [7], where it was shown that the lattice constant, bulk modulus, and cohesive energy obtained with a norm-conserving RRKJ-type [28] GGA pseudopotential were in good agreement with experimental and other first-principles calculations.

The most stable phase of WC has the HCP crystal structure, with alternating W and C layers arranged in an ABAB... stacking sequence along the $\langle 0001 \rangle$ direction [13]. In order to gauge the significance of the W 4p semi-core states, we have performed calculations on WC using both ultrasoft-type [29,42] (US) (in which the p states are treated via partial-core corrections [43]) and "all electron" projector augmented wave (PAW) pseudopotentials [44,45] (pp's). Total energies were carefully checked for convergence with respect to **k**-points and plane wave cutoff energy; it was found that 50 **k**-points were sufficient to insure convergence to $\sim$1–2 meV/atom. To achieve the same level of accuracy, different plane wave cutoff energies were required depending on which pp was used: 290 eV for US, 400 eV for PAW. Table 1 compares our results for the lattice constants, bulk modulus, and cohesive energy to that of experiment [13,46–52] and another first-principles LDA–LCAO calculation [53]. Within the GGA, we find that use of the PAW results in only minor changes to the US values. [4] As a second comparison, Fig. 1 shows the WC GGA band structure evaluated using both the US and PAW pp's. The two methods agree very well for the occupied states (virtually to within the plot resolution of the band lines), although there is some deviation for the

[4] In fact, use of the PAW leads to slightly *worse* agreement with experiment in terms of the lattice constants and cohesive energy.

Table 1
Comparison of WC bulk properties: LDA vs. GGA and ultra-soft pseudopotentials vs. the projector augmented wave method. Experimental data and another first-principles calculation (based on a linear combination of atomic orbitals) are also presented

XC	Pseudopotential	a (Å)	c (Å)	c/a	V_0 (Å^3)	B_0 (GPa)	E_{coh} (eV)
	PAW	2.932	2.849	0.972	21.21	365	16.87
GGA	Ultra-soft	2.920	2.840	0.973	20.98	375	16.67
LDA	Ultra-soft	2.881	2.802	0.973	20.15	418	19.70
	LCAO[a]	2.88	2.81	0.977	20.18	413	17.8
Experimental		2.91[b]	2.84[b]	0.976[b]	20.83	329[c], 577[d], 434[e], 443[f]	16.7[g]

[a] Ref. [53].
[b] Ref. [13].
[c] Ref. [47].
[d] Ref. [46].
[e] Refs. [49,50].
[f] Ref. [48,50].
[g] Estimated as in Refs. [51–53].

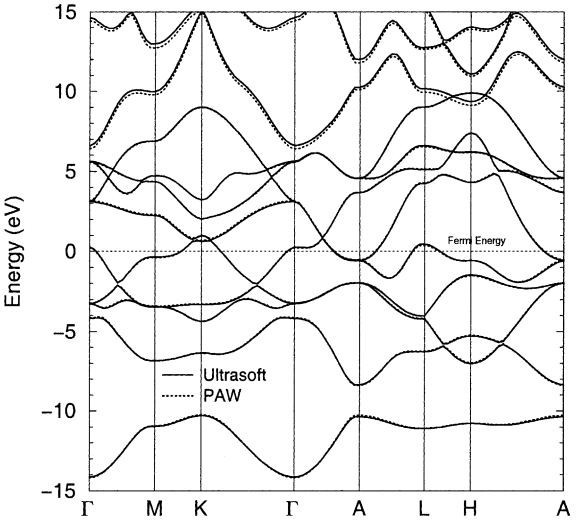

Fig. 1. Comparison of WC band structure as calculated using ultra-soft (solid lines) and PAW (dotted lines) pseudopotentials.

higher-lying unoccupied bands. Since the PAW is more computationally expensive, and since our tests show little—if any—loss of accuracy upon using the US pp's, we used the US pp's for the remainder of this work.

Table 1 also illustrates that the GGA more accurately reproduces the experimental lattice constants and cohesive energy of WC, as compared to the LDA. On average, the GGA lattice constants are less than 0.2% larger than experiment, whereas the LDA values are about 1.2% too small. These trends are consistent with the "overbinding" commonly found in LDA calculations. Although the GGA bulk modulus is roughly 10% less than that predicted within the LDA, [5] because of the large scatter in the experimental data (possibly due to poor sample characterization) it is not possible to ascertain which method is more accurate in this regard. Overall, we conclude that the GGA yields the best agreement with experiment, and our remaining calculations are therefore performed at the GGA level of theory.

Although the electronic structure of WC has been analyzed via first-principles methods by other groups (see Ref. [53] and references therein), we present here a brief review of these properties in order to facilitate comparisons with what is found at our Al/WC interfaces. Generally, the bonding in WC can be classified as a combination of metallic, ionic, and covalent (or, equivalently, as a mixture of polar covalent and metallic). The metallic aspect can be attributed to the partially filled W d bands, as evident in the band structure (Fig. 1) or, more readily, in the partial density of states [6] (pDOS)

[5] A similar discrepancy was observed in Ref. [7] for both Al and α-Al_2O_3.

[6] The Wigner-Seitz radii for evaluation of the angular momentum-projected DOS were set at: $r_W = 1.6$ Å, $r_C = 0.96$ Å, and $r_{Al} = 1.51$ Å.

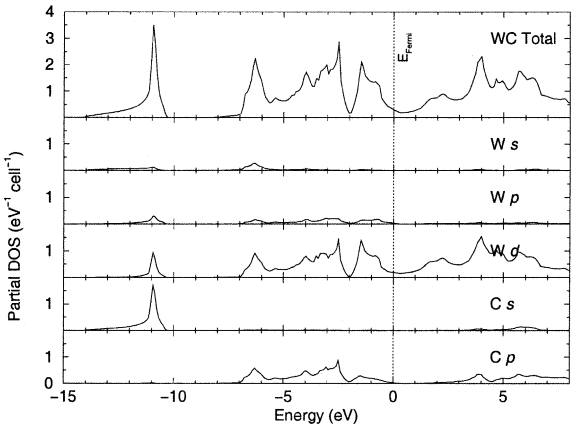

Fig. 2. Total and angular momentum projected DOS for bulk WC.

(Fig. 2). Further evidence of metallic bonding is present in the difference charge density of Fig. 3, where there is a delocalized region of charge accumulation in the interstitial regions. The ionic nature of the W–C bond is also most clearly revealed in Fig. 3, as a substantial amount of charge density centered on the W atoms is transferred to the more electronegative C atoms upon formation of the carbide. Lastly, the presence of a covalent interaction is indicated by the similar energy position and shape of the pDOS (Fig. 2) for the C p (and to a lesser extent, s) and W d states.

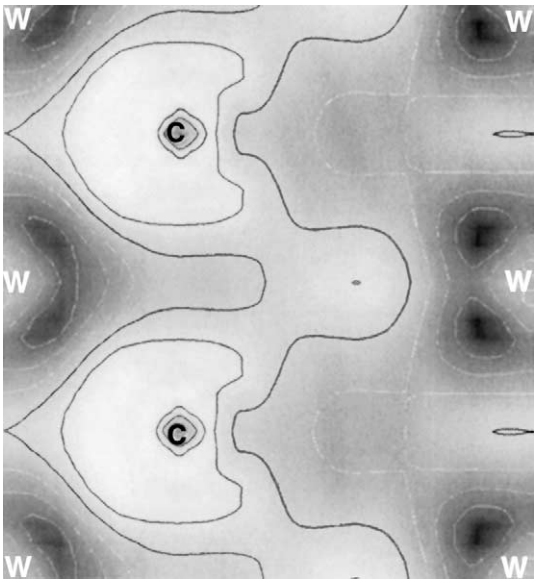

Fig. 3. WC difference charge density (relative to the isolated atoms) through a $(11\bar{2}0)$ slice intersecting both W and C atoms. Charge redistribution is visualized by a grey scale scheme in which lighter shades (black contour lines) indicate charge accumulation, and darker shades (white contours) indicate charge depletion.

3.2. Surface properties

3.2.1. Convergence tests

The purpose of this study is to simulate the interface between two *bulk-like* slabs. It is therefore necessary to insure that the slabs used are sufficiently think so as to exhibit bulk-like interiors, as it is known that the adhesion properties of thin films can differ significantly from those of thicker structures. To these ends, we have conducted convergence tests on the Al(1 1 1) and WC(0 0 0 1) slabs in preparation for their use in interface calculations.

In a previous paper [7], we presented results for the convergence of the Al(1 1 1) surface. We found that a relatively small slab consisting of only five atomic layers was sufficient to converge the surface energy and relaxations of the first two interlayer spacings. Good agreement was obtained between our PW91 prediction of the surface energy (0.81 J/m^2), and that from experiment [54,55]: 0.82 J/m^2, scaled to 0 K for the (1 1 1) surface. We have adopted that slab geometry in this study.

The $(1 \times 1)(0\,0\,0\,1)$ (basal) surface of WC is classified as a polar surface since its terminal surface layer consists of a single species of C anions or W cations. Experimentally, this surface has been known to have a catalytic activity similar to Pt and Pd, and as such has been the focus of several experimental [56–61] and theoretical [62] investigations. The basal geometry poses some practical difficulties in determining the surface energy in the context of a supercell-based electronic structure calculation. That is, for a stoichiometric slab it is not possible to terminate both surfaces of the slab with the same species. In addition, an asymmetric geometry induces a spurious dipole moment within the supercell [63], which can bias atomic forces and energies. A solution to this problem can be

achieved by using a symmetric slab. This eliminates dipole effects, and allows the calculation of the surface energy (for a specific termination) by assuming a reasonable range of values for the C and W chemical potentials [64] (see the following section). By using a symmetric slab it is also possible to check for the presence of a bulk-like interior without requiring a surface energy calculation.

Our tests on WC(0 0 0 1) were performed using both C- and W-terminated slabs ranging from 3 to 13 layers thick. Additional **k**-point convergence tests revealed that 10 irreducible **k**-points were needed to converge the total energy to ~1–2 meV/atom. A 10 Å vacuum region was also included in the supercells to prevent interactions between periodic images, and all atomic coordinates were optimized to a force tolerance of 0.05 eV/Å per atom. We used three metrics to check for the presence of a bulk-like interior with respect to slab thickness, n: the work function ϕ, surface relaxations Δ_{ij}, and the total energy. Table 2 shows that ϕ converges rapidly with slab thickness, to within 0.1 eV for $n \geqslant 7$. For the W-termination we find $\phi \simeq 5.3$ eV, and for the C-termination $\phi \simeq 6.2$ eV. These values are in good agreement with those found by the unrelaxed LAPW calculations of Mattheiss and Hamann [62] (5.2 eV W-term, 6.4 eV C-term), which were performed within the LDA using symmetric nine-layer slabs.

Table 3 compares the relaxations of the first few interlayer spacings Δ_{ij} as a function of slab thickness, n. Both terminations exhibit an oscillatory expansion/contraction behavior as one moves deeper into the slab (i.e., for increasing values of ij), and the contraction of the first layer of the C-terminated surface ($\Delta_{12} = -22.5\%$) is much larger than that found for the W-termination ($\Delta_{12} = -4.2\%$). We are unaware of any experimental or first-principles calculations with which to compare these results. As a final check on the agreement between pp's, we compared the US and PAW relaxations (see column 9:PAW) for the nine-layer C-terminated slab, and good agreement was obtained. Similar to our findings for the work function, Table 3 shows that relaxations up to the third interlayer (Δ_{34}) are well converged for $n \geqslant 7$. Lastly, we examined the change in total energy ΔE for increasingly thicker slabs. For slabs with $n \geqslant 7$ we found that ΔE was within 0.01 eV of the bulk energy per WC unit of −22.40 eV. Taken as a

Table 2
Convergence of the work function ϕ with slab thickness for W- and C-terminated WC(0 0 0 1)

# Layers, n	ϕ (eV)	
	C-term	W-term
3	6.62	–
5	5.90	5.46
7	6.22	5.35
9	6.14	5.36
11	6.24	5.31
13	6.17	5.28

Table 3
WC(0 0 0 1) surface relaxations as a function of termination and slab thickness

Termination	Interlayer	Slab thickness, n						
		3	5	7	9	9:PAW	11	13
C	Δ_{12}	−21.8	−23.2	−22.5	−22.5	−21.8	−22.5	−22.5
	Δ_{23}		4.2	5.6	5.6	7.7	5.6	5.6
	Δ_{34}			−2.1	−2.1	−2.1	−2.8	−2.1
	Δ_{45}				0	0.7	0.7	0.7
	Δ_{56}						0	0
	Δ_{67}							0.7
W	Δ_{12}	−3.5	−4.2	−4.2	−4.2	–	−4.2	−4.2
	Δ_{23}		1.4	1.4	1.4	–	2.1	2.1
	Δ_{34}			0.7	0	–	0	0
	Δ_{45}				0.7	–	0.7	0.7
	Δ_{56}						0	0
	Δ_{67}							0

Units are percentage of bulk interlayer spacing.

whole, these three tests consistently show that slabs with $n \geqslant 7$ possess a bulk-like interior and are therefore suitable for use in interface studies.

3.2.2. Stability

Due to the symmetry of WC(0 0 0 1) it is not possible to calculate an absolute surface energy without resorting to a thermodynamic argument that accounts for the effects of non-stoichiometry. Since the stoichiometric slab has two different surfaces—one C-terminated, and one W-terminated—a non-stoichiometric model with identical surfaces must be used to extract the surface energy of a particular termination. The generalized definition of the surface free energy is then given by: σ [64–66]:

$$\sigma = \frac{1}{2A}(E_{\text{slab}} - N_{\text{W}}\mu_{\text{W}} - N_{\text{C}}\mu_{\text{C}} + PV - TS). \qquad (2)$$

Here E_{slab} is the total energy of a fully relaxed, nine-layer W- or C-terminated slab, A is the surface area, μ_{W} and μ_{C} are the chemical potentials of W and C, respectively, and N_{W} and N_{C} are the numbers of the corresponding atoms in the supercell. At 0 K and typical pressures, the PV and TS terms may be neglected. Furthermore, as the surface is assumed to be in equilibrium with the bulk, the chemical potential of the bulk carbide (μ_{WC}(bulk)), its 0 K heat of formation (ΔH_{f}^0), and the elemental bulk chemical potentials (μ_{W}(bulk), μ_{C}(bulk)) are related by:

$$\mu_{\text{WC}}(\text{bulk}) = \mu_{\text{W}} + \mu_{\text{C}}, \qquad (3)$$

$$\mu_{\text{WC}}(\text{bulk}) = \mu_{\text{W}}(\text{bulk}) + \mu_{\text{C}}(\text{bulk}) + \Delta H_{\text{f}}^0. \qquad (4)$$

ΔH_{f}^0 is defined as:

$$\Delta H_{\text{f}}^0 = \mu_{\text{WC}}(\text{bulk}) - [\mu_{\text{C}}(\text{bulk}) + \mu_{\text{W}}(\text{bulk})]. \qquad (5)$$

In addition, the chemical potential for each species must be less than the chemical potential in its bulk phase:

$$\mu_{\text{W}} \leqslant \mu_{\text{W}}(\text{bulk}) \quad \text{and} \quad \mu_{\text{C}} \leqslant \mu_{\text{C}}(\text{bulk}), \qquad (6)$$

otherwise the compound would be unstable to decomposition into the elemental phases. In reality, there may be other compounds of different stoichiometry that further restrict the allowable range of μ_i values. For example, W_2C has a smaller (less negative) ΔH_{f}^0 than WC, so WC would likely transform into W_2C before the bulk phases separate. Although it is conventional [64] to use the wider range of μ_i (i.e., with respect to the bulk phases), our results (Fig. 4) also indicate the regime where W_2C is stable.

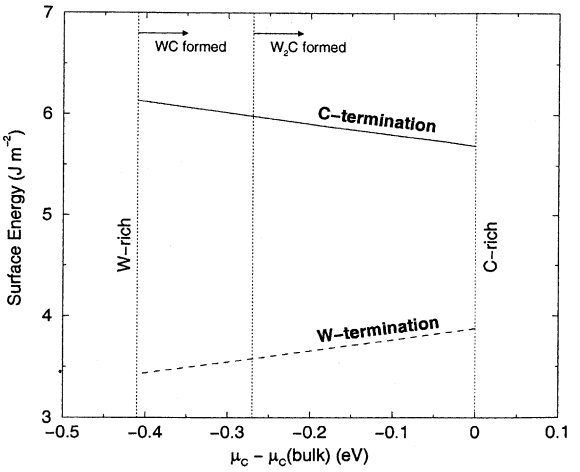

Fig. 4. Surface energy vs. chemical potential for W- and C-terminated WC(0 0 0 1) surfaces. Vertical lines indicate the range of stability of WC and W_2C.

Using the above relationships (Eqs. (3)–(6)), it is possible to rewrite Eq. (2) in terms of μ_{C} only:

$$\sigma = \frac{1}{2A}(E_{\text{slab}} - N_{\text{W}}\mu_{\text{WC}}(\text{bulk}) + (N_{\text{W}} - N_{\text{C}})\mu_{\text{C}}). \qquad (7)$$

Eq. (6) is plotted in Fig. 4 for both C- and W-terminations vs. $\mu_{\text{C}} - \mu_{\text{C}}$(bulk) for the range given by:

$$\Delta H_{\text{f}}^0 \leqslant \mu_{\text{C}} - \mu_{\text{C}}(\text{bulk}) \leqslant 0. \qquad (8)$$

Values for μ_{WC} and μ_{C} were taken from separate converged bulk calculations, and ΔH_{f}^0 was determined to be -0.41 eV, in good agreement with the available (room temperature) experimental value [67] of -0.42 eV. [7] Calculations on bulk W were performed on the primitive BCC cell using a plane

[7] Low temperature experimental thermodynamic data for WC is not available.

wave cutoff of 320 eV and 84 **k**-points in the irreducible Brillouin zone. These parameters resulted in a total energy convergence of ~1 meV/atom. For our estimate of μ_C(bulk) we used the diamond phase, which is only 0.025 eV/atom higher in formation enthalpy [67] than the (more stable) graphite phase. The total energy of the two atom primitive cell was converged to ~1 meV/atom upon using a 300 eV cutoff energy and 35 **k**-points. Both calculations yielded good agreement with experimental bulk modulus and lattice constant data.

As shown in the Fig. 4, our calculations predict that the W-termination has the lowest surface energy by about 2–2.6 J/m^2 over the entire range. In addition, the absolute values of both surface energies are relatively large, as one would expect from a polar surface. In particular, because the bonding in WC is partially ionic, cleaving along the basal plane breaks strong cation–anion bonds. This is energetically very unfavorable, and results in very reactive surfaces with large surface energies. As will be shown below, these reactive surfaces also impact interfacial adhesion energies.

4. Interfaces

4.1. Model geometry

Our model of the Al/WC interface uses a superlattice geometry in which a nine-layer WC(0 0 0 1) slab is placed between two five-layer slabs of Al(1 1 1) (generating a 19 atom supercell), resulting in two identical interfaces per supercell. The free surfaces of the Al slabs are separated by 10 Å of vacuum, and additional **k**-point tests showed that 37 sampling points were necessary to converge the total energy of the interface system to ~1–2 eV/atom. In addition to interfacing the close-packed planes, the slabs were rotated about an axis normal to the interface so as to also align the close-packed directions, resulting in the orientation relationship:

$$\mathrm{Al}[\bar{1}10](111) \quad \| \quad \mathrm{WC}[11\bar{2}0](0001). \tag{9}$$

Using this orientation, there is a modest mismatch of 2.2% between the larger WC surface unit cell and that of the Al. To accommodate the periodic boundary conditions inherent in a supercell calculation, we invoke the coherent interface approximation [68] in which the (softer) Al is stretched to match the dimensions of the carbide. In a realistic interface, the mismatch would likely result in a widely separated array of misfit dislocations, hence our model mimics the coherent regions between dislocations.

To identify the optimal interface geometry we performed a search over two parameters, resulting in six distinct candidate interface structures. The first parameter was surface termination, in which the interfacial layer of WC was terminated by either W or C atoms. Secondly, we examined three stacking sequences (or rigid shifts of the slabs in the plane of the interface), placing the interfacial Al atoms in three high-symmetry positions with respect to the WC lattice structure (see Fig. 5). Adhesion energies and interfacial energies were then calculated for all six systems, both before and after allowing for atomic relaxations.

4.2. Work of adhesion

Our estimates of the ideal work of adhesion ($\mathscr{W}_{ad}$) were calculated using two different methods. The first is based on the universal binding energy relation (UBER) [69], and involves calculating the total energy of an unrelaxed interface (formed by joining truncated bulk surfaces) as the interfacial separation is reduced from an initially large value. The ab initio data is then fit to the UBER function, yielding the optimal $\mathscr{W}_{ad}$ and interfacial separation, d_0 (see Fig. 6). The optimal geometries from the UBER calculations were then used to begin a second series of calculations in which the structure of each interface and isolated slabs were optimized via minimization of the atomic forces to a tolerance of 0.05 eV/Å. [8] To facilitate cancelation of errors between the interface models and interface vs. surface calculations, the same super-

[8] Due to the symmetry of the supercell, all atomic relaxations were along a direction perpendicular to the interface only, and all in-plane forces were equal to zero.

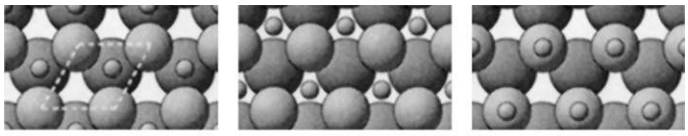

Fig. 5. Three stacking sequences for the C-terminated Al/WC interface. Small spheres: Al interfacial atoms, medium-sized spheres: C atoms, large spheres: W atoms. The supercell profile along $\langle 000\bar{1} \rangle$ is shown in white.

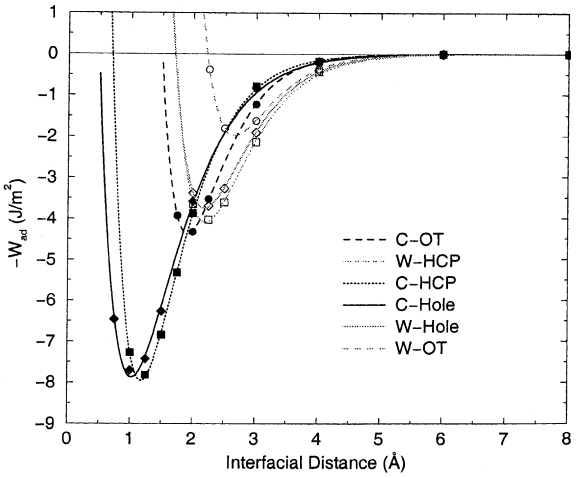

Fig. 6. Universal binding energy curves for the six Al/WC interface geometries.

cell dimensions and **k**-points were used for all calculations.

Table 4 summarizes the optimal d_0 and W_{ad} values for all six interface structures, including both the unrelaxed (UBER) and relaxed geometries. Consistent with the argument that surfaces with larger surface energies are more reactive, and therefore more readily form bonds, we see that the C-terminated interfaces exhibit larger W_{ad} values for each stacking sequence. The HCP stacking yields the largest adhesion for both terminations, with relaxed values of 6.01 J/m^2 (C-term.) and 4.08 J/m^2 (W-term.). Also, the more strongly bound C-term. has an interfacial separation of 1.21 Å—more than 1 Å smaller than that for the W-term. The HCP geometry is preferred as it comes closest to continuing the carbide's bulk ABAB... stacking across the interface and into the metal; a similar effect was also observed for the Al/α-Al_2O_3 interface [7]. The on-top (OT) site is the least favorable structure, while the hole site falls between, but somewhat closer to the HCP W_{ad}. Unfortunately, we are not aware of any experimental data with which to compare our theoretical W_{ad} values.

In the event that experimental data for the wetting of WC by Al were to become available, one would need to exercise caution in making a direct comparison to our calculated W_{ad} values. In particular, while our (1×1) model interfaces and WC surfaces may be relevant for estimates of W_{ad}

Table 4
Unrelaxed and relaxed adhesion energies (W_{ad}) and interfacial separations (d_0) for the six Al/WC interface systems. Also, W_{ad} calculated for cleavage of the clean interface within the Al, between the interfacial and subinterfacial layers

Stacking	Termination	Unrelaxed (UBER)		Relaxed	
		d_0 (Å)	W_{ad} (J/m^2)	d_0 (Å)	W_{ad} (J/m^2)
HCP	C	1.18	7.96	1.21	6.01
Hole	C	1.03	7.88	1.11	5.40
OT	C	1.92	4.37	1.98	3.21
HCP: Al cleave					2.42
HCP	W	2.20	4.09	2.22	4.08
Hole	W	2.19	3.75	2.21	3.90
OT	W	2.66	1.98	2.68	1.96
HCP: Al cleave					2.29

in *non-equilibrium* processes such as machining, under equilibrium conditions (such as in a sessile drop experiment) the WC(0 0 0 1) surface is known to reconstruct [60]. This effect would lower the surface energy and W_{ad} for the interfaces (see Eq. (1)) relative to our predictions. More information regarding the distinction between equilibrium and non-equilibrium estimates of W_{ad} can be found in Ref. [65].

Because this interface is characterized by relatively little atomic relaxation, the UBER interfacial distances are in good agreement (to within 0.1 Å) with those obtained after relaxation. Generally, we find that allowing for relaxation increases the equilibrium UBER separation, and in most cases reduces W_{ad}. The largest changes upon relaxation occur to the W_{ad} for the C-termination, which change by as much as 2.5 J/m^2. This can be explained by the energetically and structurally large relaxations present in the isolated C-terminated WC slab ($\Delta_{12} = -22.5\%$). These relaxations are about five times those found for the W-termination ($\Delta_{12} = -4.2\%$).

Table 5 shows the change in interlayer spacing (relative to bulk) for both relaxed HCP terminations as a function of distance away from the interface. Similar to what was seen in the clean surface, the WC spacings undergo an oscillatory contraction/expansion relaxation. However, the magnitude of the relaxations is much smaller in the interface, and exhibit a maximum deviation from bulk of less than 3%. This reduction is consistent with a return to a more bulk-like bonding environment as a consequence of interfacing with the Al. On the other hand, the Al spacings, although similarly small, undergo uniform contraction. This is at odds with the oscillatory behavior present in the free Al(1 1 1) surface [7,70], and is an artifact of the tensile strain imposed by the coherent interface approximation.

Table 5
Interlayer spacing with respect to position perpendicular to the interface, given in terms of absolute distance (Å) and as a percentage of the respective bulk spacing (shown in parentheses)

Interlayer	Interlayer distance (Å) (% of bulk)	
	C-term	W-term
Al_{2-3}	2.27 (−2.8)	2.23 (−4.3)
Al_{1-2}	2.32 (−0.7)	2.31 (−1.0)
Interface	1.21	2.22
WC_{1-2}	1.39 (−1.9)	1.38 (−2.7)
WC_{2-3}	1.43 (+0.9)	1.45 (+2.0)
WC_{3-4}	1.41 (−0.6)	1.42 (−0.2)
WC_{4-5}	1.43 (+0.5)	1.43 (+0.8)

The central layer of the Al slab is denoted Al_3, the interfacial Al layer as Al_1, the central WC layer is WC_5, etc.

One feature common to strongly bound interfaces is the phenomenon of adhesive metal transfer. This occurs during tensile loading of the interface, wherein interfacial failure occurs *within* one of the slabs comprising the interface, as opposed to at the interface proper. A portion of the fractured slab's material is then transferred to the other slab. In essence, the interfacial bonds (i.e., adhesive strength of the interface) are stronger than the cohesive strength of one of the interfaced materials. To assess whether adhesive metal transfer is a possibility for the Al/WC system, we have performed additional W_{ad} calculations on the optimal W-HCP and C-HCP geometries. This was done by separating the interface within the softer Al between the interface and subinterface layer (see Table 4 under the heading "Al cleave"). We find that both interface terminations are subject to cleavage within the metal—to the extent that dissipative effects like plastic deformation can be neglected—as the calculated W_{ad} of 2.3–2.4 J/m^2 within Al are much less than that for separation at the original metal/ceramic junction: 6.01 J/m^2 (C-term), and 4.08 J/m^2 (W-term). The possibility of adhesive metal transfer suggests that the polar Al/WC interface would not be an optimal choice for use in tribological applications such as dry machining or other applications requiring weak bonding between carbide and metal.

As a final comment on the accuracy of DFT adhesion energies, we note that it has recently been shown [71,72] that both LDA and GGA underestimate surface energies with respect to experiment or "exact" computational methods. Although we do not see such an effect in the case of Al(1 1 1) (see Section 3.2.1, and we are unaware of any experimental (or exact theoretical) data for WC(0 0 0 1), this would suggest that our predicted adhesion energies were roughly 5–10% too small based on the jellium calculations of Ref. [72].

In conclusion, we find that the $\mathscr{W}_{ad}$ for both (optimal) HCP terminations is relatively large, which is consistent with the polar nature of the WC(0 0 0 1) surface. This large adhesion indicates a likelihood for adhesive metal transfer, as $\mathscr{W}_{ad}$ values calculated within the Al slab are substantially smaller than those found at the Al/carbide junction.

4.3. Stability analysis

Apart from knowing $\mathscr{W}_{ad}$ for a particular interface, it is also desirable to know which interface is most stable in a thermodynamic sense. This can be assessed in a manner similar to what was done for the WC surface, by extending Eq. (7) to give the interfacial free energy [8], γ:

$$\gamma = \frac{1}{2A}\{E_{int} - N_W\mu_{WC} + (N_W - N_C)\mu_C - N_{Al}\mu_{Al}(bulk)\} - 2\sigma_{Al}. \quad (10)$$

Here $2\sigma_{Al}$ is the surface energy of the two free Al(1 1 1) surfaces, and $\mu_{Al}(bulk)$ is the chemical potential of bulk Al. Based on this, Fig. 7 plots the interface free energy for all six interface geometries as a function of $\mu_C - \mu_C(bulk)$.

Although the C-HCP interface has the largest $\mathscr{W}_{ad}$, its large surface energy results in the W-termination having a lower interfacial free energy, except for a small region within the C-rich regime. [9] Neglecting such effects as defect segregation, our calculations therefore predict that the W-termination should be the preferred equilibrium termination for the regime in which WC is favorable.

4.4. Electronic structure

To reveal the nature of the interfacial bonding between metal and ceramic, Figs. 8–10 depict the interfacial charge density difference, its planar average along $\langle 0\,0\,0\,1\rangle$, and the layer-projected DOS, respectively, for the relaxed W-HCP and C-HCP

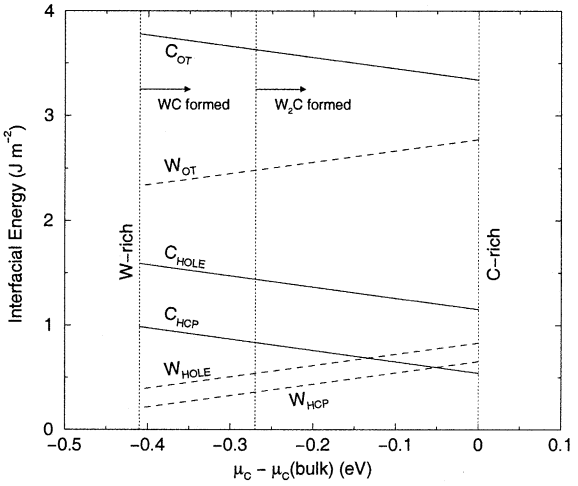

Fig. 7. Interfacial free energy for the six Al/WC geometries as a function of $\mu_C - \mu_C$(bulk).

interfaces. The difference charge density was evaluated with respect to the isolated slabs according to the relation:

$$\rho(\boldsymbol{r})_{interface} - [\rho(\boldsymbol{r})_{Al(1\,1\,1)} + \rho(\boldsymbol{r})_{WC(0\,0\,0\,1)}], \quad (11)$$

and is visualized in Fig. 8 using the same grey-scale scheme used in Fig. 3. The slice is oriented along $(1\,1\,\bar{2}\,0)$, and those atoms intersected by the slicing plane are identified.

Despite their different terminations, there are some features of the interfacial electronic structure common to both systems. First of all, Fig. 8 shows that the interfacial charge redistribution is a localized effect, being confined to within the first Al layer, and either the first (W-HCP) or second layer (C-HCP) in the carbide. This conclusion is supported by the DOS plot of Fig. 10, where the subinterface DOS are similar to their values in the center of their respective slabs. Secondly, there are extended regions of charge depletion in the interstitial regions of the interfacial Al layer, as can be seen both in Figs. 8 and 9. This signals a reduction in lateral Al–Al metallic bonding in favor of forming new bonds across the interface.

In addition to these similarities, there are also significant differences in the interfacial bonding characteristics of the two terminations. Considering

[9] In this region WC is unstable to decomposition into W_2C.

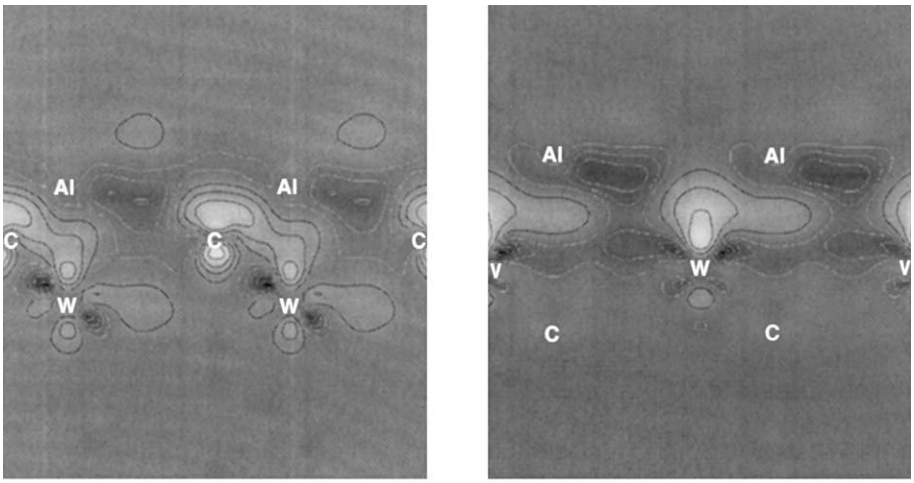

(a) C-HCP (b) W-HCP

Fig. 8. Charge density difference (relative to the isolated surfaces) for the C-HCP and W-HCP interfaces taken along the $(11\bar{2}0)$ direction. The color scheme is the same as in Fig. 3, and the locations of the interfacial atoms are labeled.

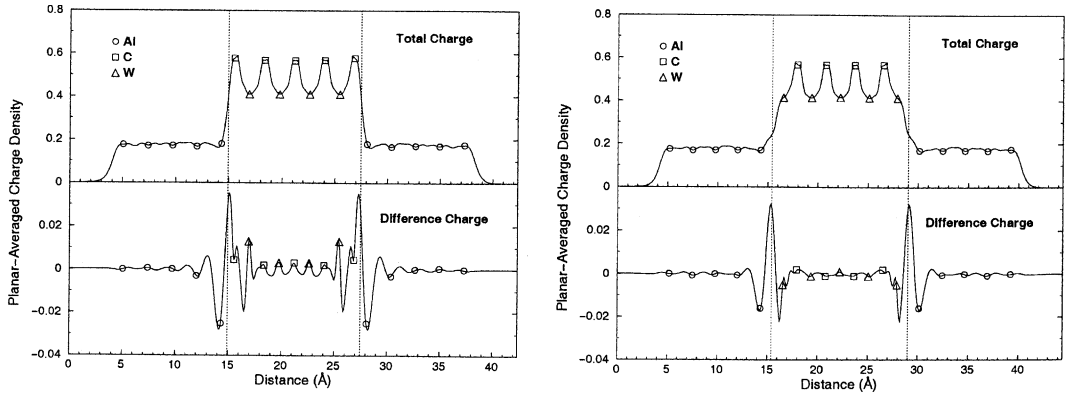

(a) C-HCP (b) W-HCP

Fig. 9. Planar-averaged total charge and charge density difference (relative to the isolated surfaces) for the C-HCP and W-HCP geometries along a direction normal to the interfaces.

the W-HCP system first, we note in Fig. 8b a depletion of charge in the lateral W–W interfacial bonds similar to what is observed for the Al interfacial layer. This combination of charge density (from both the W and Al lateral bonds) is pushed into the interfacial region forming what roughly appears to be a mixed covalent/metallic bond involving a W d_{z^2} orbital. Further evidence for this can be seen in Fig. 9b where there is charge depletion on both the interfacial W and Al layers, coincident with a large increase in the interface region indicating a possible covalent/metallic bond. Lastly, the interfacial DOS (Fig. 10b) for the Al and W layers do not display any prominent

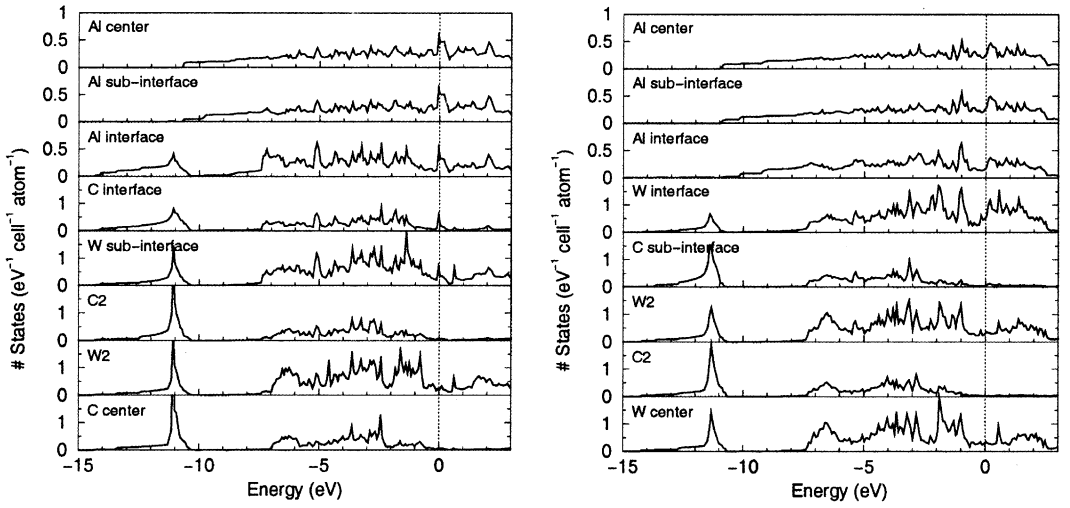

(a) C-HCP (b) W-HCP

Fig. 10. Layer-projected DOS for the C-HCP and W-HCP interfaces.

features suggestive of a strong covalent interaction. Rather, the Al interface DOS is slightly perturbed in a fashion similar to the shape of its nearest-neighbor W atom with a similar trend observed for the W, as its DOS begins to look more free electron like. We therefore interpret the W-HCP interfacial bond to be a combination of a weakly covalent and strong metallic interaction involving only the interfacial W d-states and Al 3sp states.

In contrast to the metallic/covalent character of the W-HCP system, the more strongly bound C-HCP interface exhibits a mix of covalent and ionic bonding (equivalently, polar covalent bonding). The effect of the interface also extends further into the carbide, as the d states on the subinterface W atoms now participate in charge redistribution (see Fig. 8a). The depletion of W–W lateral bonding within the carbide's interfacial layer seen for the W-HCP system is not present for the C–C bonds in the C-HCP interfacial layer. Instead, Fig. 8a suggests a charge transfer from the Al interfacial layer to a C p_z orbital, and to a lesser extent a d_{z^2} orbital on the subinterface W atom. This ionic-like effect is also visible in Fig. 9a, where the planar average of the charge difference shows charge depletion on the interfacial Al layer, accompanied by charge accumulation on the C and W interface atom. [10] However, the layer-resolved DOS for the C-HCP system (Fig. 10a) indicates that the charge-transfer from metal to carbide is not complete, and there remains some degree of covalent bonding. In particular, there is a new set of Al 3sp–C 2s overlap states in the -14 to -10 eV range on the interfacial Al and C atoms. In addition, there is a depletion of states on the Al in the -10 to -7 eV range and in the region near the Fermi level (E_F). This depletion roughly mimics the behavior of the C p DOS. Lastly, although the C atoms in the carbide bulk have a vanishing DOS near E_F, the presence of metallic Al at the interface induces new C gap states near E_F. Overall, the C-HCP DOS shows a much stronger covalent interaction than seen in the W-HCP system, due to formation of Al–C bonds. The partially ionic nature of this interface explains its larger W_{ad} compared to the W-termination.

[10] We attempted to quantify the charge transfer by integrating the Wigner–Seitz spheres on each atom, but found the results to be inconclusive due to intersphere overlap and incomplete space filling.

4.5. Alloy effects on adhesion

It is known that segregation of alloying agents to surfaces and grain boundaries (GB's) can significantly impact the mechanical properties, corrosion resistance, etc. of Al alloys [73,74]. Although, most modern alloys (for example, the 5xxx series) contain several alloying agents in various amounts, Mg and Li are the dominant segregants to surfaces and GB's as a result of their larger atomic size. (Mg and Li are, respectively, 12% and 6% larger than Al.) Assuming a similar preference for segregation to interfaces, we have conducted a small set of ab initio calculations to determine how Li and Mg alter W_{ad} with respect to the clean interfaces. Other mechanisms [75], such as the reduction of Al_2O_3 by Mg to form MgO, may play a significant role in determining the overall effect of interfacial segregation on W_{ad}.

Table 6 shows the relaxed interfacial separations (d_0) and W_{ad} values for the W-HCP and C-HCP interfaces assuming a substitutional monolayer of Li or Mg atoms replacing the interfacial Al layer. As in the clean interfaces, all atomic forces were minimized to a tolerance of 0.05 eV/Å. For both terminations we find that the presence of Li and Mg reduces W_{ad} and increases d_0—i.e., the impurity atoms weaken the interface. The reduction in W_{ad} is largest for the C-HCP system, where W_{ad} decreases by 2.5 and 1.7 J/m^2, respectively, for Li and Mg. For W-HCP the decrease in W_{ad} is smaller: 2.1 (Li) and 1.5 J/m^2 (Mg). The smaller effect on the W-HCP system can be explained by its larger d_0 of 2.22 Å of the clean interface, vs. 1.21 Å for the C-HCP geometry: the W-HCP geometry initially has more free volume to accommodate the larger impurity atoms, and expands less upon their addition. This behavior suggests that strain effects play an important role in determining the effects of impurities on W_{ad}. Nonetheless, strain effects are not the only factor at work, as can be seen by comparing the reduction in W_{ad} from Li with that from Mg. If strain effects alone were responsible for the changes in adhesion, then the larger Mg atoms should reduce W_{ad} the most. However, just the opposite behavior is seen, with Li having a stronger effect, suggesting that electronic contributions are also significant. The trend in interface separation more closely follows the behavior expected from a strain-only effect, as d_0 is largest for the Mg-containing structures. We note that an earlier study [76] of the effects of impurity atoms on metal/ceramic adhesion involving C and S impurities at the Al(1 0 0)/MgO and Ag(1 0 0)/MgO interfaces found that, in general, impurities reduced W_{ad}.

Table 6
Changes in W_{ad} due to the substitutional incorporation of Li and Mg at the Al surface

Termination	d_0 (Å)	W_{ad} (J/m^2)
C: clean	1.21	6.01
C: Li	1.42	3.50
C: Mg	1.46	4.31
W: clean	2.22	4.08
W: Li	2.36	1.98
W: Mg	2.39	2.58

5. Summary and conclusions

We have presented the first ab initio study of metal–ceramic adhesion involving the Al–WC interface. We have focused on the polar Al(1 1 1)/WC(0 0 0 1) geometry due to its relatively small misfit, and a future paper will investigate the nonpolar Al(1 1 0)/WC(1 1 $\bar{2}$ 0) system and draw comparisons. Considerable care was taken to ensure that the thickness of the slabs utilized were sufficient to allow for a bulk-like interface. We find that both the clean WC surface and Al/WC interface are W-terminated, as these structures have the lowest surface and interfacial free energies. Overall, interface adhesion is relatively strong, with the optimal C- and W-terminations yielding W_{ad} values of 6.01 and 4.08 J/m^2, respectively. These values can be rationalized in terms of the large surface energies obtained for the polar surfaces. By cleaving along (0 0 0 1) one creates a very reactive surface by breaking cation–anion bonds, and leaving behind a terminating layer with a large surface dipole. Despite the strong interfacial bonding, there are only small changes in the atomic structure at the interface; interlayer spacings in both the metal and the carbide are relatively close to their bulk values. Moreover, the optimal adhe-

sion site for both terminations places the interfacial metal atoms in the HCP site with respect to the carbide stacking sequence. This geometry effectively continues the carbide crystal structure into the metal, an effect which has also been seen for the Al/α-Al_2O_3 system [7].

To further explain the trends in W_{ad}, we critically analyzed the electronic structure of both the C-HCP and W-HCP interfaces by referring to the charge density and layer-projected DOS. For both terminations the interface-induced changes in the electronic structure are very short ranged and limited to the first (in the metal) or second (in the carbide) interfacial layers. The W-HCP system is characterized by a mixture of metallic and covalent bonding, whereas the stronger bound C-HCP interface exhibits polar covalent interactions, with charge transfer to the interfacial C layer.

Lastly, we considered the effects of Li and Mg alloying agents on W_{ad}. Consistent with their large size, we find that both reduce W_{ad} by 1.5–2.5 J/m^2, and push the C-HCP and W-HCP interface apart, suggesting that strain effects are important. However, electronic effects are also significant, as the smaller Li impurities generate a larger reduction to W_{ad}—a result which cannot be explained in terms of strain effects alone.

Acknowledgements

Computational resources were provided by the National Computational Science Alliance at the University of Illinois at Urbana-Champaign under grant MCA96N001N. Financial support was provided by the National Science Foundation Division of Materials Research under grant DMR9619353. D. Siegel acknowledges General Motors Corp. for financial support during a summer internship.

References

[1] M.W. Finnis, J. Phys.: Condens. Mat. 8 (1996) 5811.
[2] D.M. Lipkin, D.R. Clarke, A.G. Evans, Acta Mater. 46 (1998) 4835.
[3] M.D. Kriese, N.R. Moody, W.W. Gerberich, Acta Mater. 46 (1998) 6311.
[4] J.R. Rice, in: T. Yokobori, T. Kawasaki, J. L. Swedlow (Eds.), Proceedings of the 1st International Conference on Fracture, Sendai, Japan, Jap. Soc. for Strength & Fracture of Mater., 1966, pp. 309–340.
[5] F. Rao, R. Wu, A.J. Freeman, Phys. Rev. B 51 (1995) 10052.
[6] A. Bogicevic, D.R. Jennison, Phys. Rev. Lett. 82 (1999) 4050.
[7] D.J. Siegel, L.G. Hector Jr., J.B. Adams, Phys. Rev. B, in press.
[8] W. Zhang, J.R. Smith, Phys. Rev. Lett. 85 (2000) 3225.
[9] R. Benedek, A. Alavi, D.N. Seidman, L.H. Yang, D.A. Muller, C. Woodward, Phys. Rev. Lett. 84 (2000) 3362.
[10] Y.F. Zhukovskii, E.A. Kotomin, P.W.M. Jacobs, A.M. Stoneham, Phys. Rev. Lett. 84 (2000) 1256.
[11] R. Schweinfest, S. Köstlmeier, F. Ernst, C. Elsässer, T. Wagner, Philos. Mag. A 81 (2001) 927.
[12] A. Christensen, E.A. Carter, J. Chem. Phys. 114 (2001) 5816.
[13] L.E. Toth, Transition Metal Carbides and Nitrides, Academic Press, New York, 1971.
[14] P. Hohenberg, W. Kohn, Phys. Rev. 136 (1964) B864.
[15] W. Kohn, L.J. Sham, Phys. Rev. 140 (1965) A1133.
[16] P. Alemany, Surf. Sci. 314 (1994) 114.
[17] L. Wenchang, Z. Kaiming, X. Xide, Phys. Rev. B 45 (1992) 11048.
[18] S. Li, R.J. Arsenault, P. Jena, J. Appl. Phys. 64 (1988) 6246.
[19] J. Hartford, Phys. Rev. B 61 (2000) 2221.
[20] S.V. Dudiy, J. Hartford, B.I. Lundqvist, Phys. Rev. Lett. 85 (2000) 1898.
[21] J. Hoekstra, J. Kohyama, Phys. Rev. B 57 (1998) 2334.
[22] S. Ogata, H. Kitagawa, J. Jpn. Inst. Met. 60 (1996) 1079, translation from Japanese.
[23] N. Eustathopoulos, M.G. Nicholas, B. Drevet, Wettability at High Temperatures, Pergamon Press, Amsterdam, 1999.
[24] L. Ramqvist, Int. J. Powder Metall. 1 (1965) 2.
[25] J.V. Naidich, Prog. Surf. Membr. Sci. 14 (1981) 353.
[26] D.J. Siegel, L.G. Hector Jr., J.B. Adams, in preparation.
[27] G. Kresse, J. Furthmüller, Phys. Rev. B 54 (1996) 11169.
[28] A.M. Rappe, K.M. Rabe, E. Kaxiras, J.D. Joannopoulos, Phys. Rev. B 41 (1990) 1227.
[29] G. Kresse, J. Hafner, J. Phys.: Condens. Mat. 6 (1994) 8245.
[30] W.H. Press, S.A. Teukolsky, W.T. Vetterling, B.P. Flannery, Numerical Recipes in FORTRAN 90: The Art of Parallel Scientific Computing, second ed., Cambridge University Press, Cambridge, 1996.
[31] E. Polak, Computational Methods in Optimization, Academic Press, New York, 1971.
[32] P. Pulay, Chem. Phys. Lett. 73 (1980) 393.
[33] C.G. Broyden, Math. Comput. 19 (1965) 577.
[34] D.D. Johnson, Phys. Rev. B 38 (1988) 12807.
[35] H.J. Monkhorst, J.D. Pack, Phys. Rev. B 13 (1976) 5188.
[36] N.D. Mermin, Phys. Rev. 137 (1965) A1441.
[37] M. Methfessel, A.T. Paxton, Phys. Rev. B 40 (1989) 3616.

[38] H. Hellmann, Einfuhrung in die Quantumchemie, Deuticke, Leipzig, 1937.
[39] R.P. Feynman, Phys. Rev. 56 (1939) 340.
[40] J.P. Perdew, A. Zunger, Phys. Rev. B 23 (1981) 5048.
[41] J.P. Perdew, J.A. Chevary, S.H. Vosko, K.A. Jackson, M.R. Pederson, D.J. Singh, C. Fiolhais, Phys. Rev. B 46 (1992) 6671.
[42] D. Vanderbilt, Phys. Rev. B 41 (1990) 7892.
[43] S.G. Louie, S. Froyen, M.L. Cohen, Phys. Rev. B 26 (1982) 1738.
[44] P.E. Blöchl, Phys. Rev. B 50 (1994) 17953.
[45] G. Kresse, D. Joubert, Phys. Rev. B 59 (1999) 1758.
[46] V.P. Zhukov, V.A. Gubanov, Solid State Commun. 56 (1985) 51.
[47] H.L. Brown, P.E. Armstrong, C.P. Kempter, J. Chem. Phys. 45 (1966) 547.
[48] W. Voigt, Lehrbuch der Kristalphysik, Teubner, Leipzig, 1928.
[49] A. Reuss, Z. Angew. Math. Mech. 9 (1929) 55.
[50] M. Lee, R.S. Gilmore, J. Mater. Sci. 17 (1982) 2657.
[51] E.K. Storms, The Refractory Carbides, Academic Press, New York, 1967.
[52] C. Kittel, Introduction to Solid State Physics, sixth ed., Wiley, New York, 1986.
[53] A.Y. Liu, R.M. Wentzcovitch, M.L. Cohen, Phys. Rev. B 38 (1988) 9483.
[54] W.R. Tyson, Can. Metall. Q. 14 (1975) 307.
[55] W.R. Tyson, W.A. Miller, Surf. Sci. 62 (1977) 267.
[56] R.B. Levy, M. Boudart, Science 181 (1973) 547.
[57] J.E. Houston, G.E. Laramore, R.L. Park, Science 185 (1974) 258.
[58] P.M. Stefan, M.L. Shek, I. Lindau, W.E. Spicer, L.I. Johansson, F. Herman, R.V. Kasowski, G. Brogen, Phys. Rev. B 29 (1984) 5423.
[59] K.L. Håkansson, H.I.P. Johansson, L.I. Johansson, Phys. Rev. B 49 (1994) 2035.
[60] M. Göthelid, E. Janin, J. Phys.: Condens. Matter 11 (1999) 773.
[61] J. Brillo, R. Sur, H. Kuhlenbek, H.-J. Freund, Surf. Sci. 397 (1998) 137.
[62] L.F. Mattheiss, D.R. Hamann, Phys. Rev. B 30 (1984) 1731.
[63] J. Neugebauer, M. Scheffler, Phys. Rev. B 46 (1992) 16067.
[64] K. Rapcewicz, B. Chen, B. Yakobson, J. Bernholc, Phys. Rev. B 57 (1998) 7281.
[65] I. Batyrev, A. Alavi, M.W. Finnis, Faraday Discuss. 114 (2000) 33.
[66] W. Zhang, J.R. Smith, Phys. Rev. B 61 (2000) 16883.
[67] R.C. Weast, CRC Handbook of Chemistry and Physics, 67th ed., CRC Press, Boca Raton, FL, 1983.
[68] R. Benedek, D.N. Seidman, M. Minkoff, L.H. Yang, A. Alavi, Phys. Rev. B 60 (1999) 16094.
[69] J.R. Smith, T. Hong, D.J. Srolovitz, Phys. Rev. Lett. 72 (1994) 4021.
[70] J. Schöchlin, K.P. Bohnen, K.M. Ho, Surf. Sci. 324 (1995) 113.
[71] K. Carling, G. Wahnström, T.R. Mattsson, A.E. Mattsson, N. Sandberg, G. Grimvall, Phys. Rev. Lett. 85 (2000) 3862.
[72] Z. Yan, J.P. Perdew, S. Kurth, C. Fiolhais, L. Almeida, Phys. Rev. B 61 (2001) 2595.
[73] X.-Y. Liu, P.P. Ohotnicky, J.B. Adams, C.L. Rohrer, R.H. Hyland Jr., Surf. Sci. 373 (1997) 357.
[74] X.Y. Liu, J.B. Adams, Acta Mater. 46 (1998) 3467.
[75] K. Wefers, Aluminum 57 (1981) 722.
[76] T. Hong, J.R. Smith, D.J. Srolovitz, Acta Metall. Mater. 43 (1995) 2721.